Journal of Structural Biology 172 (2010) 319–330

Contents lists available at ScienceDirect

Journal of Structural Biology

journal homepage: www.elsevier.com/locate/yjsbi

Solution structure and phospho-PmrA recognition mode of PmrD from *Klebsiella pneumoniae*

Shih-Chi Luo [a,b,c], Yuan-Chao Lou [b], Hsin-Yao Cheng [d], Yun-Ru Pan [b,c], Hwei-Ling Peng [d], Chinpan Chen [a,b,*]

[a] *Chemical Biology and Molecular Biophysics, Taiwan International Graduate Program, Academia Sinica, Taipei 115, Taiwan*
[b] *Institute of Biomedical Science, Academia Sinica, Taipei 115, Taiwan*
[c] *Institute of Bioinformatics and Structural Biology, National Tsing Hua University, Hsinchu 300, Taiwan*
[d] *Department of Biological Science and Technology, National Chiao Tung University, Hsinchu 300, Taiwan*

ARTICLE INFO

Article history:
Received 15 April 2010
Received in revised form 3 June 2010
Accepted 4 June 2010
Available online 9 June 2010

Keywords:
NMR
SPR
PmrD connector protein
Chemical shift perturbation
Saturation transfer
BeF_3^- activation

ABSTRACT

In bacteria, the two-component system (TCS) is the most prevalent for sensing and transducing the environmental signals into the cell. In *Salmonella*, the small basic protein PmrD is found to protect phospho-PmrA and prolong the expression of PmrA-activated genes. In contrast, *Escherichia coli* PmrD fails to protect phospho-PmrA. Here, we show that *Klebsiella pneumoniae* PmrD (*KP*-PmrD) can inhibit the dephosphrylation of phospho-PmrA, and the interaction between *KP*-PmrD and the N-terminal receiver domain of PmrA ($PmrA_N$) is much stronger in the presence than in the absence of the phosphoryl analog beryllofluoride (BeF_3^-) ($K_D = 1.74 \pm 0.81$ μM vs. $K_D = 236 \pm 48$ μM). To better understand the molecular interactions involved, the solution structure of *KP*-PmrD was found to comprise six β-strands and a flexible C-terminal α-helix. Amide chemical shift perturbations of *KP*-PmrD in complex with BeF_3^--activated $PmrA_N$ suggested that *KP*-PmrD may undergo a certain conformational rearrangement on binding to activated $PmrA_N$. Saturation transfer experiments revealed the binding surface to be located on one face of the β-barrel. This finding was further verified by *in vivo* polymyxin B susceptibility assay of the mutants of *KP*-PmrD. The phospho-PmrA recognition surface of *KP*-PmrD, which involves two *KP*-PmrD proteins in complex with an activated-$PmrA_N$ dimer, is suggested to be a contiguous patch consisting of Trp3, Trp4, Ser23, Leu26, Glu27, Met28, Thr46, Leu48, Ala49, Asp50, Ala51, Arg52, Ile65, Asn67, Ala68, Thr69, His70, Tyr71, Ser73 and Glu74. Our study furthers the understanding of how PmrD protects phopho-PmrA in the PmrAB TCS.

1. Introduction

Hundreds of two-component systems (TCSs) have been found in eubacteria, archaea, and a few eukaryotic organisms (Wurgler-Murphy and Saito, 1997). The TCS is the most prevalent system in bacteria for transducing external information into the cell and for coping with environmental stresses (Hoch, 1995; Stock et al., 2000). The TCS is composed of a membrane-spanning sensor histidine kinase (HK) and a cytoplasmic response regulator (RR). The commonly accepted mechanism of TCS is that the sensor kinase is autophosphorylated at a conserved His residue in its cytosolic kinase domain in response to an extra- or intra-cellular signal detected by its sensor domain. Subsequently, the phosphoryl group is transferred to an Asp residue in the receiver domain of the intra-cellular cognate RR, often resulting in modulation of gene expression for suitable adaptation. In *Salmonella*, the PmrAB TCS governs inducible resistance to the cationic antibiotic polymyxin B (Groisman et al., 1997) by responding to high Fe^{3+} and low Mg^{2+} signals (Groisman, 2001). At high Fe^{3+} levels, the sensor kinase PmrB undergoes autophosphorylation, then the phosphoryl group is transferred to the cognate response regulator PmrA (Wosten et al., 2000). At low Mg^{2+} concentrations, the signal is transduced from the sensor protein PhoQ to its cognate response regulator PhoP, which increases the transcription of *pmrD* gene (Kox et al., 2000). The resulting PmrD protein binds to the phospho-PmrA and protects it against dephosphorylation, thus prolonging the active state of PmrA for the persistent expression of its downstream genes (Kato and Groisman, 2004). The PmrD protein hence modifies the signaling and therefore is an important player

Abbreviations: PmrD, polymyxin B resistance protein D; *KP*, *Klebsiella pneumonia*; *KP*-PmrD, *Klebsiella pneumonia* PmrD; C35S, point mutation of *KP*-PmrD from cystein to serine at residue 35; TCS, two-component system; HK, histidine kinase; RR, response regulator; $PmrA_N$, the N-terminal receiver domain of PmrA; BeF_3^-, the phosphoryl analog beryllofluoride; NMR, nuclear magnetic resonance; SPR, surface plasma resonance; HX_NOEs, Heteronuclear NOEs; HSQC, heteronuclear single quantum coherence; NOE, nuclear Overhause enhancement; NOESY, nuclear Overhause enhancement spectroscopy.

* Corresponding author at: Institute of Biomedical Sciences, Academia Sinica, 128 Academia Rd., Section 2, Taipei 115, Taiwan. Fax: +886 2 2788 7641.
E-mail address: bmchinp@ibms.sinica.edu.tw (C. Chen).

1047-8477/$ - see front matter © 2010 Elsevier Inc. All rights reserved.
doi:10.1016/j.jsb.2010.06.007

overall in two-component signaling in *Salmonella*. The solution structure of *Escherichia coli* PmrD has been reported (Fu et al., 2007). However, the *E. coli* PmrD fails to protect phospho-PmrA in inducing the expression of the PmrA-activated genes (Winfield and Groisman, 2004).

Klebsiella pneumoniae (*KP*), a Gram-negative bacterium, is a common cause of hospital-acquired infections worldwide, including pneumonia, urinary tract diseases, and bacteremia, particularly in immuno-compromised patients (Prince et al., 1997). PmrD in *K. pneumoniae* (*KP*-PmrD) consists of 81 amino acids and shows 44% and 35% sequence identity with *Salmonella* and *E. coli* PmrD, respectively (Fig. S1). The PmrD protein belongs to a new class of proteins named TCS connectors, which use different mechanisms of action for signal integration of bacterial cellular processes (Mitrophanov and Groisman, 2008). However, the phospho-PmrA recognition mode of PmrD is not understood and the broad interest in the PmrD proteins has led us to study details of the molecular interactions involved.

In this paper, we present the solution structure of *KP*-PmrD and show that it can inhibit the dephosphorylation of phospho-PmrA. We investigated the strength of interactions between *KP*-PmrD and the N-terminal receiver domain of PmrA ($PmrA_N$) in the presence and absence of the phosphoryl analog beryllofluoride (BeF_3^-) (Cho et al., 2001; Yan et al., 1999) through surface plasma resonance (SPR) and NMR techniques. By exploiting the chemical shift perturbations combined with the saturation transfer techniques, residues that form direct intermolecular contacts could be separated from residues that undergo conformational changes. The phospo-PmrA recognition mode of *KP*-PmrD was suggested and verified by site-directed mutagenesis for *in vivo* polymyxin B susceptibility assay. The structural characteristics of *KP*-PmrD that enable it to stabilize the phospho-PmrA are discussed.

2. Materials and methods

2.1. Cloning, expression, and purification of the recombinant proteins

The coding regions of *pmrD*, *pmrA*, and *pmrA*$_N$ (the N-terminal 130 residues) were PCR amplified from the genomic DNA of *K. pneumoniae*. The amplified gene products were cloned as an *Nde*I/*Xho*I fragment into the pET29b vector (Novagene). The resulting plasmids (pET-PmrD, pET-PmrA, and pET-$PmrA_N$) allowed for the in-frame fusion of each coding region containing an additional LEHHHHHH sequence at the C terminus to facilitate protein purification. The recombinant proteins were overexpressed in the host *E. coli* strain BL21(DE3) (Novagen) induced with 1 mM IPTG at 37 °C (for *KP*-PmrD) or 30 °C (PmrA or $PmrA_N$). After lysis with use of an M-110S microfluidizer (Microfluidics) and subsequent centrifugation, the overproduced proteins were purified from the soluble fraction by affinity chromatography on His-Bind resin (Novagene) and size-exclusion chromatography with a Superdex75 10/300 GL column. The eluted samples were dialyzed against 20 mM Na_2HPO_4 (pH 6.0), 30 mM NaCl and concentrated by using an Amicon (MW 5000; Millipore). For isotopically enriched samples, cells were grown in M9 minimal medium (Sambrook et al., 1989) containing 1 g/L $^{15}NH_4Cl$ and 2 g/L ^{13}C glucose. The DNA fragments harboring the coding region of *pmrB*$_{C276}$ (the cytoplasmic domain of PmrB) were PCR amplified from the genomic DNA of *K. pneumoniae* and cloned as a *Bam*HI/*Hin*dIII fragment into pET30b (Novagen). The recombinant proteins $PmrB_{C276}$ were overproduced in *E. coli* BL21 (DE3) induced by 0.5 mM IPTG at 37 °C and purified as described above. The C35S mutant was generated according to the QuikChange™ (Stratagene) protocol. The authenticities of the recombinant proteins were verified by SDS–PAGE and mass spectrometry analysis.

2.2. In vitro phospho-transfer assay

The *in vitro* phospho-transfer assay was performed essentially as described (Kato and Groisman, 2004). The phospho-$PmrB_{C276}$ was obtained by pre-incubating $PmrB_{C276}$ protein (5 μM) with 40 μCi [γ-^{32}P]ATP in 80 μl of 1× phosphorylation buffer (10 mM Tris–HCl pH 7.5, 138 mM NaCl, 2.7 mM KCl, 1 mM $MgCl_2$, and 1 mM DTT) for 1 h at room temperature. The reaction mixture was then chilled on ice, and 5 μl of the mixture was removed and mixed with 2.5 μl of 5 × SDS sample buffer as a reference sample. The phospho-$PmrB_{C276}$ protein mixture (30 μl) was then mixed with equal volumes of 1× phosphorylation buffer containing PmrA (10 μM) or PmrA with *KP*-PmrD (each at 10 μM) to initiate the phospho-transfer reaction. Aliquots of 10-μl were removed at specific time points and mixed with 2.5 μl of 5 × SDS sample buffer to stop the reaction. These samples were kept on ice until SDS–PAGE. After electrophoresis at 4 °C, the signal was detected by autoradiography.

2.3. Size-exclusion chromatography

Size-exclusion chromatography was performed by use of a high-performance liquid chromatography AKTA system (Amersham Biosciences) with a Superdex75 10/300 GL column. Experiments were carried out at room temperature at a flow rate of 0.3 ml/min with 20 mM Tris–HCl, 50 mM NaCl (pH 7.0) as the mobile phase while monitoring absorbance at 280 nm. Loading concentrations of 50 and 400 μM were used for *KP*-PmrD and $PmrA_N$, respectively. Each analysis was performed with a 300 μl aliquots. Samples containing 150 μg *KP*-PmrD and 1800 μg $PmrA_N$ were prepared with or without BeF_3^- (35 mM NaF, 7 mM $MgCl_2$, 5.3 mM $BeCl_2$, and 10 mM 2-ME).

2.4. Real-time binding kinetics

Real-time kinetic analysis of *KP*-PmrD bound with $PmrA_N$ involved use of a Biacore 3000 biosensor system (Biacore, Uppsala, Sweden). Carboxymethylated sensor chips (type CM5) were activated with a 1:1 mixture of 0.2 M *N*-ethyl-*N*′-(3-dimethylaminopropyl) carbodiimide and 50 mM *N*-hydroxysuccinimide in water. *KP*-PmrD [10 μg/ml in 30 mM NaCl, 20 mM NaH_2PO_4 (pH 6.0)] was immobilized on the sensor chips by amide coupling (Biacore). Unreacted sites on the chip were blocked with 1 M ethanolamine (pH 8.5). SPR signals from the immobilized *KP*-PmrD generated about 200 Biacore response units. Control flow cells were activated and blocked in the absence of *KP*-PmrD protein. Binding was evaluated over ranges of $PmrA_N$ concentrations (0.032–4 μM) in buffer A [0.05% Tween 20, 30 mM NaCl, 20 mM NaH_2PO_4 (pH 6.5)] under continuous flow of 30 μl/min at 25 °C. $PmrA_N$ in the presence of BeF_3^- was achieved by adding 5.3 mM $BeCl_2$ (Fluka), 35 mM NaF, and 7 mM $MgCl_2$. Binding of $PmrA_N$ to *KP*-PmrD-immobilized flow cells was corrected for observed binding to control flow cells. The resulting sensorgrams were analyzed by use of BIAevaluation software v4.1.

2.5. Circular dichroism spectra

CD experiments involved use of an Aviv 202 SF CD spectrometer (Lakewood, NJ) calibrated with (+)-10-camphorsulfonic acid (CSA) at 25 °C. *KP*-PmrD was diluted to a final concentration of 20 μM in 50 mM NaH_2PO_4, 50 mM NaCl at the desired pH. For far-UV CD spectra, a 1-mm path-length cuvette was used, and the spectra were recorded three times from 190 to 260 nm with a wavelength step of 0.5 nm. Thermal denaturation experiments involved monitoring changes in ellipticity at 210 nm from 5 °C to 95 °C with a 2 °C interval and 2 min for equilibrium. For the chemical denaturation experiment, guanidine hydrochloride (Gdn·HCl) was used

and the change of molar ellipticity at 210 nm was monitored with 5 μM *KP*-PmrD in 50 mM NaH_2PO_4 (pH 6.0) and 50 mM NaCl in a 1-cm path-length cuvette at 25 °C. After background subtraction and smoothing, all CD data were converted from CD signals (millidegree) to mean residue ellipticity (deg cm^2 $dmol^{-1}$). The curves were fitted and analyzed by use of SigmaPlot 8.02 (SPSS Inc.).

2.6. NMR resonance assignments and structure determination of KP-PmrD

NMR experiments on 0.4 mM ^{15}N, ^{13}C-labeled or ^{2}H, ^{15}N-labeled *KP*-PmrD in 20 mM NaH_2PO_4 (pH 6.0) and 30 mM NaCl in a Shigemi NMR tube (Allison Park. PA, USA) were carried out at 298 K with use of Bruker AVANCE 600 and 800 NMR spectrometers (Bruker, Karlsruhe, Germany) equipped with a triple (^{1}H, ^{13}C, and ^{15}N) resonance cryoprobe including a shielded z-gradient. All heteronuclear NMR experiments were performed as described in a review article (Kay, 1995). Sequence-specific assignment of the backbone atoms was achieved by independent connectivity analysis of CBCA(CO)NH, HNCACB, HNCO, and HN(CA)CO. Assignment of ^{1}H resonances involved 3D total correlation spectroscopy (TOCSY)-heteronuclear single quantum coherence (HSQC), 3D nuclear Overhauser effect spectroscopy (NOESY)-HSQC, HAHB(CO)NH, and HCCH-TOCSY. The combined information from 2D ^{1}H–^{15}N HSQC and 3D NOESY-HSQC experiments yielded assignments for side-chain amide resonances of the Asn and Gln residues. All NMR spectra were processed with the NMRPipe package (Delaglio et al., 1995) and analyzed by use of NMRView 5.0 (Bruce and Richard, 1994). NMR structures were calculated from experimental restraints by simulated annealing with the program Xplor-NIH. The dihedral angle information was predicted by use of TALOS (Gabriel et al., 1999). The hydrogen bonding information was obtained from D_2O exchange monitored by the ^{1}H–^{15}N HSQC spectra. The final 20 structures with no distance restraint violation greater than 0.3 Å and no dihedral angle restraint violations larger than 3° were chosen on the basis of the total energy. The quality of the structures was analyzed by use of PROCHECK-NMR (Roman et al., 1996). The chemical shifts of *KP*-PmrD at pH 6.0 and 298 K were deposited in BioMagResBank under accession number BMRB-11063. The best 20 structures, together with the complete list of restraints, were deposited in the Brookhaven Protein Data Bank under accession number 2RQX.

2.7. Chemical shift perturbation experiments

To map the binding sites on *KP*-PmrD with non-activated or BeF_3^--activated $PmrA_N$, we collected a series of ^{1}H–^{15}N HSQC spectra of $^{2}H/^{15}N$-labeled *KP*-PmrD with and without 5.3 mM $BeCl_2$ (Fluka), 35 mM NaF, and 7 mM $MgCl_2$ by increasing the amount of unlabeled $PmrA_N$ at molar ratios (*KP*-PmrD/$PmrA_N$) of 0, 0.76, 1, 1.49, and 2. We investigated and ruled out the possibility that the shift changes of *KP*-PmrD were due to constituents of BeF_3^-. All spectra processing were analyzed by use of XWIN-NMR (Bruker Biospin) and analyzed by use of SPARKY (Goddard and Kneller, 2001). Normalized chemical shift changes were calculated as follows:

$$\Delta\delta = [\Delta H^2 + (0.17\Delta N)^2]^{1/2} \quad (1)$$

The cut-off (0.1 ppm) was set as the standard deviation for all chemical shift changes. All residues with values above the cut-off were considered affected by interaction with $PmrA_N$.

2.8. Saturation transfer experiments

Saturation transfer experiments were performed at 298 K on a Bruker AV800 spectrometer with a cryogenic probe. ^{2}H, ^{15}N-labeled *KP*-PmrD (0.4 mM) and unlabeled $PmrA_N$ (0.8 mM) were dissolved in a buffer containing 30 mM NaCl (pH 6.0) and 90% D_2O. The deuteration percentage of *KP*-PmrD is around 70%. Hence, to avoid excitation of the *KP*-PmrD protons, the saturation pulses were centered at 3411 Hz (4.26 ppm) or 3250 Hz (4.06 ppm), where show large proton peaks from $PmrA_N$ and no peak from *KP*-PmrD. The strength of each saturating Gaussian pulse covers 54 Hz (Huang et al., 2008), which should not saturate the nearby water signals (4.7 ppm) effectively. The measurement time was 24 h, with relaxation delay of 2.2 s and saturation time of 1.2 s. The molar ratio of the ^{2}H, ^{15}N-labeled *KP*-PmrD to $PmrA_N$ was set to 1:2 to detect the bound state resonance of *KP*-PmrD with and without BeF_3^-. To evaluate the effect of the residual aliphatic protons within *KP*-PmrD, saturation transfer experiments were also carried out under the same conditions as above but without $PmrA_N$. All NMR spectra were processed and analyzed by use of XWIN-NMR/Sparky. The program PyMOL was used for presentation of the 3-D structures of *KP*-PmrD.

2.9. Construction of K. pneumoniae pmrD deletion mutant strain and the complementation plasmids

The allelic exchange strategy (Lai et al., 2003) was used to construct a chromosomal Δ*pmrD* mutant strain in *K. pneumoniae* CG43S3 (Lai et al., 2003). The resulting *K. pneumoniae* mutant was named D2906. For the complementation of *pmrD* mutation, the DNA fragments encompassing the *pmrD* gene and its 278-bp upstream region were PCR amplified and cloned into the shuttle vector pRK415 (Keen et al., 1988) to generate pRK415-PmrD. To construct *pmrD* complementation plasmids encoding PmrD with point mutations, two DNA fragments were PCR amplified from *K. pneumoniae* CG43S3 genomic DNA: one with the primer set designed complementary to *pmrD* upstream 278 bp region and to the mutation site; the other with the primer set designed complementary to the mutation site and the 3′-end of *pmrD* gene. The PCR products were mixed, diluted 100-fold individually and used as the template for a second PCR amplification with the primer set designed complementary to the *pmrD* upstream region and 3′-end of *pmrD* gene. The resulting DNA fragments, each harboring a mutant *pmrD* allele preceded by a native *pmrD* promoter region, were cloned into pRK415 to generate pRK415-PmrDL26A, -PmrDM28A, -PmrDT46A, -PmrDT77A and -PmrDN78A. All the plasmids have been confirmed by sequence analysis.

2.10. Polymyxin B susceptibility assay

Polymyxin B sulfate salt (8210 USP units per mg) (Sigma–Aldrich) was prepared as 1 unit/μl stock solution in PBS and stored at 4 °C. The bacterial resistance to polymyxin B was determined as described (Campos et al., 2004; Groisman et al., 1997) with some modifications. The overnight cultures of *K. pneumoniae* strains were washed twice with PBS, diluted 1:100 into LB medium and grown at 37 °C until absorbance of OD_{600} reached 0.7. The cells were then harvested, washed twice with PBS and diluted to approximately 2×10^4 CFU/ml in LB broth. An amount of 100 μl of the diluted culture was added to a 96-well microtiter dish preloaded with equal volumes of PBS-diluted polymyxin B at final concentrations of 0, 2, 4, 6, 8 or 10 units/ml. After incubation at 37 °C for 1 h with shaking, 100 μl of the suspension was directly plated onto LB agar plates and incubated at 37 °C overnight to determine the colony forming units of the viable cells. The relative survival rate was expressed as the percentage of colony forming units after treatment to that of those not exposed to the antimicrobial agent. For simplicity, the bacterial survival after the treatment of 4 units/ml polymyxin B was shown. Assays were performed on

at least three independent occasions, and the data were the mean and standard deviation from triplicate samples.

3. Results

3.1. KP-PmrD acts to prevent the dephosphorylation of PmrA

In *Salmonella enterica*, the phosphorylation of PmrA by the cognate sensor protein PmrB enhances its affinity in binding to its target promoter (Aguirre et al., 2000). The dephosphorylation of PmrA by PmrB helps to relieve over-activation of this system, whereas *Salmonella* PmrD protects PmrA against both intrinsic and PmrB-mediated dephosphorylation (Kato and Groisman, 2004). To verify whether *KP*-PmrD participates in the phosphorylation cascade, we performed an *in vitro* phospho-transfer assay. As shown in Fig. 1, PmrA was rapidly phosphorylated with the addition of autophosphorylated His-$PmrB_{C276}$ (lanes 2 and 9) and then gradually dephosphorylated (lanes 3–7). However, in the presence of *KP*-PmrD, the phosphorylation level of PmrA was still maintained at 60 min (lane 13) and lasted at least 4 h (lane 14). Because the same amounts of PmrA were used in the assay with and without PmrD, the above observation is unlikely to result from the change in protein turnover rate. Therefore, our results suggest that *KP*-PmrD can inhibit the dephosphorylation of PmrA from PmrB.

3.2. Assessing the binding stoichiometry of KP-PmrD and $PmrA_N$

To assess the binding stoichiometry of *KP*-PmrD and $PmrA_N$, we performed size-exclusion chromatography (SEC) and ^1H transverse relaxation time measurements. For SEC, the following molecular mass standards were used for calibration: albumin (peak a, Fig. S2) and chymotrypsinogen A (peak b, Fig. S2). The locations of *KP*-PmrD and $PmrA_N$ were confirmed by the individual free form samples (data not shown). *KP*-PmrD yields a single peak at the same retention volume as peak III of Fig. S2. This is in the proximity of the theoretical mass of a *KP*-PmrD monomer (10.4 kDa). However, $PmrA_N/BeF_3^-$ yields a single peak at the same retention volume as peak II of Fig. S2, which is close to the theoretical mass of a $PmrA_N$ dimer (30.9 kDa). At an eightfold excess of $PmrA_N$, the estimated molecular mass of the *KP*-PmrD/$PmrA_N$ protein complex (peak I, Fig. S2) is close to the predicted mass of a $PmrA_N$ dimer bound with two *KP*-PmrDs (51.7 kDa). This result was confirmed by the ^1H transverse relaxation time (T_2) measured by the 1-1 echo sequence (Anglister et al., 1993). The measured ^1H transverse relaxation times of free *KP*-PmrD, free $PmrA_N$ dimer and *KP*-PmrD/$PmrA_N$ complex in the presence of BeF_3^- were 31.3, 11.9 and 6.7 ms, which correspond to the T_2 values of spherical proteins with molecular weight around 12, 33 and 59 kDa, respectively. Therefore, both SEC and T_2 relaxation times suggested that the *KP*-PmrD/$PmrA_N$ complex sample in the presence of BeF_3^- comprises two molecules of each protein.

3.3. Binding interactions between KP-PmrD and $PmrA_N$ determined by SPR

KP-PmrD was immobilized on a CM5 sensor chip by amide coupling. Triplicate injections of $PmrA_N$ analyte in the presence or absence of BeF_3^- were performed at concentrations of 4000, 2000, 1000, 500, 250, 125, 63, and 32 nM. The resulting sensorgrams were analyzed using BIAevaluation software version 4.1. As equilibrium was achieved over the course of each injection, the equilibrium dissociation constant (K_D) was determined by plotting the response at equilibrium against analyte concentrations and fitting the data to a 1:1 binding isotherm. In the presence of BeF_3^-, $PmrA_N$ showed higher levels of responses (Fig. 2A, the maximum response is about 80 RU) with the immobilized PmrD and the fitting yielded a K_D value of 1.74 ± 0.81 μM, which is considered as a moderate strength of binding for protein–protein interactions. Kinetic parameters for the interaction were determined based on global fitting of the sensorgrams providing the association ($k_a = 5.0 \times 10^4\ M^{-1}\ s^{-1}$) and dissociation ($k_d = 7.30 \times 10^{-2}\ s^{-1}$) rate constants. The K_D value obtained from the steady-state methods (1.37 ± 0.19 μM, Fig. 2B) is close to the value determined from global fitting. This result is reassuring the 1:1 binding model in global fitting methods and presumably ruling out of some more complex binding mechanisms. In contrast, in the absence of BeF_3^-, $PmrA_N$ showed lower levels of response units (Fig. 2C, the maximum response is about 20 RU) with the immobilized *KP*-PmrD than those observed in the presence of BeF_3^-. The equilibrium dissociation constant could not be accurately fitted, since K_D value is greater than half of the highest concentration used (4 μM) based on the steady-state methods (Fig. 2D). The SPR data suggest that the strength of interactions between *KP*-PmrD and BeF_3^--activated $PmrA_N$ are much stronger than that in the absence of BeF_3^-.

3.4. NMR resonance assignment and structure description of KP-PmrD

We assigned most of the backbone and side-chain resonances of *KP*-PmrD, with the exception of Ser72, which is missing presumably because of chemical/conformational exchange broadening. The consensus chemical shift index calculated with $^1H^\alpha$, $^{13}C^\alpha$, $^{13}C^\beta$, and $^{13}C'$ chemical shifts (Wishart and Sykes, 1994) revealed that *KP*-PmrD is primarily composed of six β-strands and an α-helix at the C terminus (data not shown). From the observed cross-over NOEs, such as $d_{\alpha\alpha}(i, j)$ and $d_{\alpha N}(i, j)$ and the slowly exchanging amide protons, we confirmed that these β-strands form a 6-stranded antiparallel β-sheet (β1: Trp3-Gln9, β2: Cys17-Ser23, β3: Leu26-Glu33, β4: Lys44-Pro47, β5: Tyr53-Leu55, and β6: Thr62-Thr69). The C-terminal α-helix at Ser73-Ala79 was identified from the observation of α-helical NOEs. On the basis of $d_{\alpha\delta}(i, i+1)$ NOEs, conformations of the two proline residues (Pro47 and Pro59) were assigned as *trans*. Amide proton exchange rate study showed that most of the slowly exchanged amide protons are located in the 6-stranded antiparallel β-sheet, which indicates that

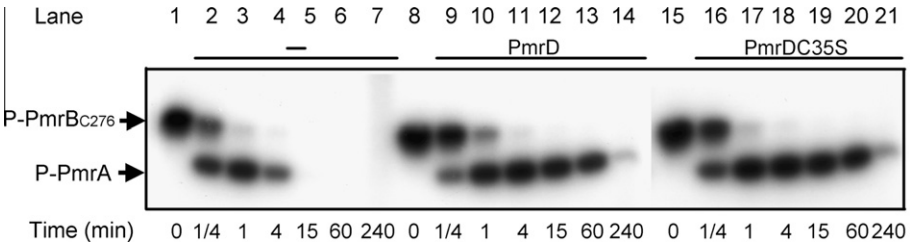

Fig. 1. *In vitro* phospho-transfer assay of wild-type *KP*-PmrD and C35S mutant. The phospho-transfer assay of PmrA (final concentration 5 μM) phosphorylated by the cognate sensor protein $PmrB_{C276}$ (final concentration 2.5 μM) was performed with or without *KP*-PmrD and C35S (final concentration 5 μM), and the phosphorylation states of PmrA and $PmrB_{C276}$ were investigated at specific time points.

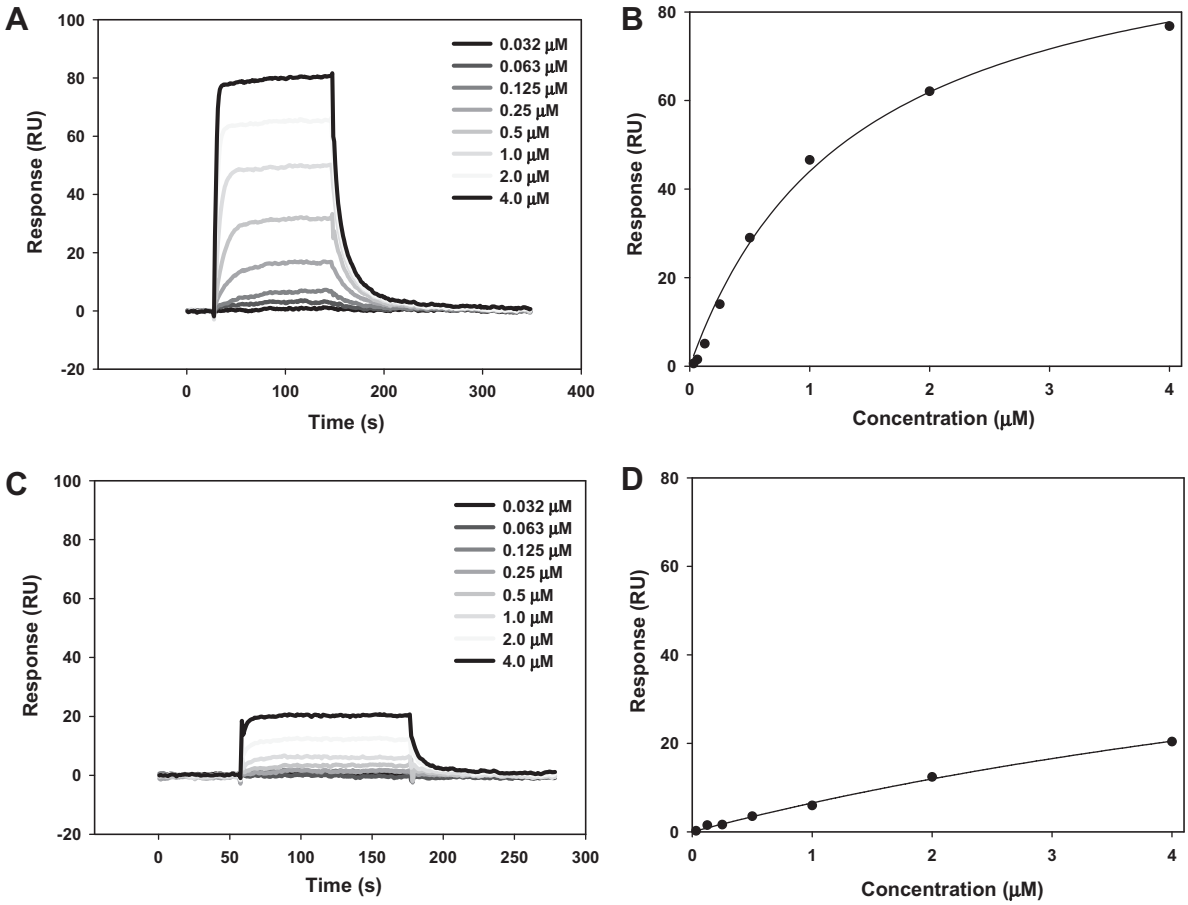

Fig. 2. Binding kinetics and strength of interactions between *KP*-PmrD and $PmrA_N$ determined by surface plasma resonance (SPR). Different concentrations of $PmrA_N$ (0.032, 0.063, 0.125, 0.25, 0.5, 1, 2, and 4 μM) with (A) and without (B) BeF_3^- were injected onto immobilized PmrD. SPR units for each experiment were overlaid against the time after injection. Plots based on the steady-state methods in SPR for $PmrA_N$ are shown with (C) and without (D) BeF_3^-.

the β-sheet conformation is more stable than the C-terminal α-helix. We generated the NMR solution structure of *KP*-PmrD on the basis of 1068 NOE restraints (213 intra, 301 sequential, 116 medium, and 438 long-range distance restraints), 30 hydrogen bond distances, and 106 ϕ/ψ dihedral angle restraints. The structural statistics of the ensemble of 20 final refined structures are summarized in Table 1. A stereo view of the ensemble (Fig. 3A) shows that

Table 1
Structural statistics for the 20 final structures of *KP*-PmrD.

Total distance restraints	1068
Intramolecular constraints ($\|i-j\|=0$)	213
Sequential constraints ($\|i-j\|=1$)	301
Medium-range constraints ($1<\|i-j\|\leqslant 4$)	116
Long-range constraints ($\|i-j\|>4$)	438
Total hydrogen bond restraints	30
Total torsion angle restraints	106
Deviations from idealized covalent geometry	
Bonds (Å)	0.0022 ± 0.00004
Angles (°)	0.2898 ± 0.0031
Impropers (°)	0.2431 ± 0.0055
RMS deviation from the mean structure (residues 2–80)	
Backbone atoms	0.5 ± 0.15 Å
Heavy atoms	1.0 ± 0.17 Å
Ramachandran data	
Residues in most favored regions (%)	71.8
Residues in additional allowed regions (%)	23.5
Residues in generously allowed regions (%)	4.7
Residues in disallowed regions (%)	0.1

KP-PmrD is mainly composed of a β-barrel structure comprised of six twisted and slightly bent antiparallel β-strands and a C-terminal α-helix. The C-terminal α-helix is packed against the β-barrel structure, and Leu55-Asn58 and Asn58-Gln61 form two short 3_{10} helices identified by the hydrogen bond of the carbonyl oxygen of residue *i* and the H^N group of residue *i* + 3. Residues Trp3, Val5, Val19, Leu21, Ile32, Leu39, Leu45, Tyr53, Leu55, Leu63, and Ile65, highly conserved for PmrD proteins from different bacteria, form the major hydrophobic core inside the β-barrel. Another smaller hydrophobic core formed by residues Val20, Ile29, and Trp76 was identified outside the β-barrel. The surface structure of *KP*-PmrD (Fig. 3B) shows that positively and negatively charged residues are exposed to the aqueous phase, with Glu33 close to Arg66, and Glu41 near to Lys6, which indicates that electrostatic forces also play a role in stabilizing the *KP*-PmrD structure.

3.5. NMR titrations for KP-PmrDC35S with non-activated or BeF_3^--activated $PmrA_N$

To improve the solubility and stability of the KP-PmrD/$PmrA_N$ complex, we designed a mutant with Cys35 replaced by Ser (C35S). This mutant shows good solubility and expression yield and hence is more suitable for NMR structural study. CD spectra of C35S and *KP*-PmrD are similar (Fig. S3A), which indicates that both proteins exhibit a similar secondary structure. Also, 2D ^1H–^{15}N HSQC spectra of C35S and *KP*-PmrD (Fig. S3B) are well superimposed, except for those near residues C17 and C35, which reveals that both proteins possess similar tertiary structures. To

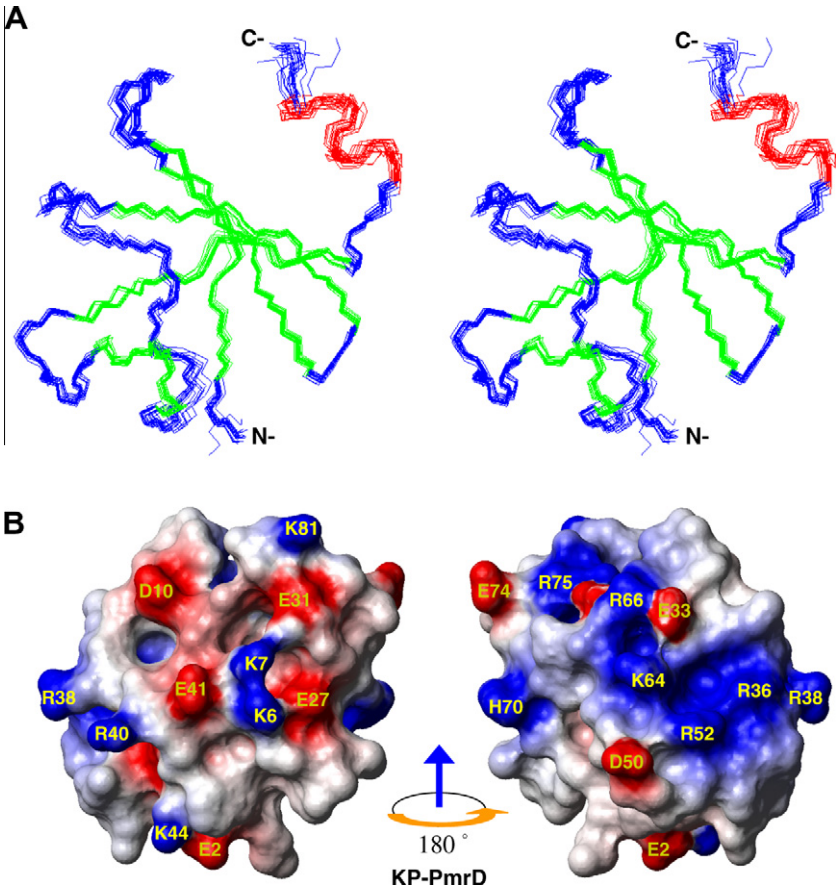

Fig. 3. NMR solution structure of *KP*-PmrD. (A) A stereo view of the ensemble of 20 NMR solution structures of *KP*-PmrD, with β-strands in green, α-helix in red and loops in blue. (B) Surface structure of *KP*-PmrD showing charge distribution with negatively and positively charged residues in red and blue, respectively, and labeled.

verify whether C35S can participate similar to *KP*-PmrD in the phosphorylation cascade, we performed the same *in vitro* phospho-transfer assay (Fig. 1). The results suggested that C35S can also specifically inhibit the dephosphorylation of PmrA by PmrB. We thus used C35S mutant to mimic *KP*-PmrD to carry out chemical shift perturbation and cross-saturation experiments. Because of the large molecular size and low solubility of the complex sample, we prepared ^{15}N, ^{2}H-labeled C35S and acquired a number of 2D ^{1}H–^{15}N HSQC spectra during the titration with unlabeled $PmrA_N$ with and without BeF_3^-.

In the absence of BeF_3^-, it is clearly seen that the chemical shift of each cross peak is the weighted average of those between the free and the bound *KP*-PmrDs (Fig. 4A), revealing the exchange is enacted in a fast exchange regime. We were able to assign most of the resonances of C35S in complex with $PmrA_N$ by tracing the shift changes during titration from ratio of C35S–$PmrA_N$ of 1:0 to 1:2 (Fig. 5A, red color). The K_D could be calculated under the assumptions of the fast exchange regime and a "one binding site model" of the interaction (Fig. S4). The averaged dissociation constant was estimated to be around 236 μM (Table 2), which is in agreement with the SPR data showing a weak interaction for *KP*-PmrD/$PmrA_N$ in the absence of BeF_3^-. However, residues Trp3, Ser23, Ala25, Ile29, Ala49, Arg52, Asn57, Asn67, Ala68, Ser73, Glu74, and Arg75 could not be assigned in a complex state because of broadening of peaks, which suggests that these residues are in an intermediate exchange regime. Also, residues Glu2, Glu31 and Trp76 could not be assigned unambiguously because of peak overlapping. The chemical shift perturbations ($\Delta\delta$) of amide resonances between the free C35S and its complex without BeF_3^- were calculated (Fig. 5B, red bar). The largest changes were seen in residues Thr69 at the end of β-strand 6 and Thr77 at the center of C-terminal α-helix. Large changes were also seen in residues Val8 and Asp10 at the end of β-strand 1 and start of loop 1. These features were shown in a ribbon structure of *KP*-PmrD, with the shift changes coded by a color gradient (Fig. 5C).

We next investigated the interactions between C35S and $PmrA_N$ in phosphorylation-mimicking conditions with BeF_3^-. In the beginning of $PmrA_N$ titration, no significant shift changes were observed. The cross peaks of C35S disappeared, broadened or had decreased intensities with the increasing amount of $PmrA_N$. At a molar ratio of 1 to 1.0, two separate NMR signals, one for the free and the other for the bound form, were detected for several residues (e.g., Thr62, and Thr77 in Fig. 4B), which indicates a slow exchange regime for C35S in complex with $PmrA_N$ in the presence of BeF_3^-, which agrees with the slow dissociation rate constant measured by SPR. An overlay of the ^{1}H, ^{15}N-HSQC spectra of the free C35S and the C35S/$PmrA_N$ complex at a molar ratio of 1 to 2.0 was produced (Fig. 5A, green color). Most of the resonances of C35S in complex with BeF_3^--activated $PmrA_N$ were assigned by comparing the assigned cross peaks for C35S with non-activated $PmrA_N$ (Fig. 5A, red color). Some cross peaks such as Trp3, Ser23, Ile29, Ala30, Ala49, Asp50, Arg52, Ile65, Asn67, Ala68, Tyr71, Ser73, Glu74, and Arg75 could not be observed, which suggests an intermediate exchange regime for these residues. Interestingly, these residues seem to locate on the same face of *KP*-PmrD (Fig. 5D, orange color). The residues exhibiting large combined (^{1}H, ^{15}N) chemical shift perturbations (>0.1 ppm) with $PmrA_N$ binding are Trp4 to Asp10, Cys17 to Ala34, Lys44 to Asn57, and Thr62 to Asn78 (Fig. 5B, black bar). To understand the binding sites of *KP*-PmrD in complex with $PmrA_N$ in the presence of BeF_3^-, we mapped these features onto the

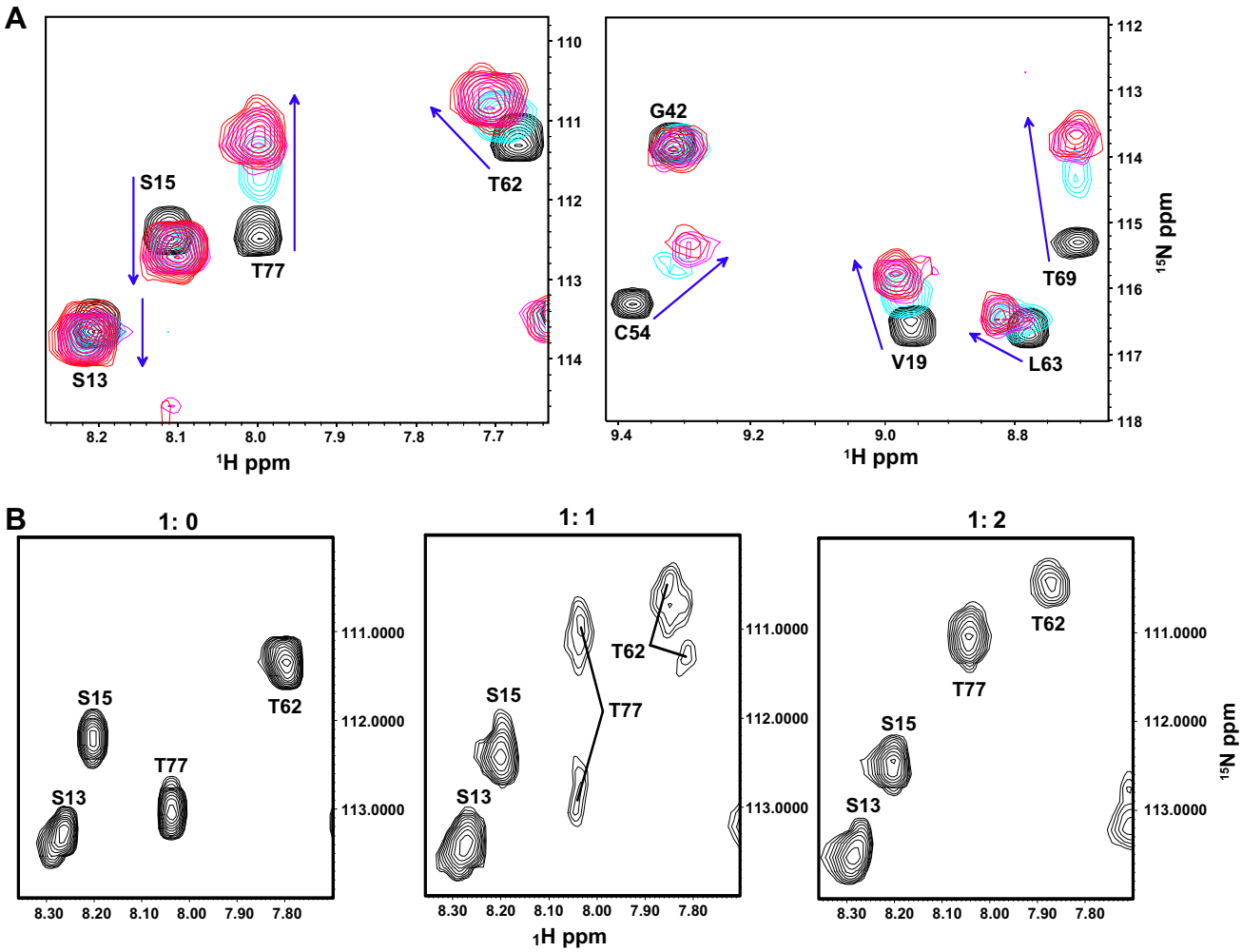

Fig. 4. Differential chemical exchange regimes in NMR observed in portions of the ^{15}N, ^{1}H heteronuclear single quantum coherence (HSQC) spectra for the interactions of *KP*-PmrD and PmrA$_N$ with and without BeF_3^-. In the absence of BeF_3^- (A), a fast exchange regime in NMR is suggested by the position of the peak, which is the weighted average of the peaks of the free and bound forms. The different colors represent 0 (black), 0.76 (cyan), 1.49 (magenta), and 2.0 (red) molar ratio of ^{15}N-labeled *KP*-PmrD to PmrA$_N$. By contrast, with BeF_3^- present during titration, a slow exchange regime in NMR (B) is suggested by the observation of two cross peaks for a subset of the residues at the 1:1 M ratio. (For interpretation of the references in color in this figure legend, the reader is referred to the web version of this article.)

ribbon of the free *KP*-PmrD structure by a color gradient (Fig. 5D, blue to red). The shifted residues lie in all secondary structural regions and constitute several discontinuous faces, which indicates that *KP*-PmrD may undergo certain conformational rearrangement on binding to activated PmrA$_N$. The binding sites on *KP*-PmrD with BeF_3^--activated PmrA$_N$ could not be easily determined by chemical shift perturbation.

3.6. Saturation transfer experiments of KP-PmrD C35S in complex with PmrA$_N$

Chemical shift changes could be due to direct protein interactions or conformational rearrangements beyond the binding sites. Therefore, to separate the direct intermolecular contacts from the residues with conformational changes, we performed NMR saturation transfer experiments (Takahashi et al., 2000). On *KP*-PmrD forming a complex with PmrA$_N$, the saturation of the proton magnetization in the PmrA$_N$ can be transferred to the interaction interface of *KP*-PmrD, therefore decreasing the intensity of the amide cross peaks in interaction sites. For this experiment, C35S was labeled uniformly with ^{2}H (>98%) and ^{15}N to avoid the excitation of aliphatic protons of C35S by the radiofrequency pulses. The labeled *KP*-PmrD was dissolved in 10% $^{1}H_2O$ and 90% $^{2}H_2O$ to decrease the saturation transfer through spatially crowded amide protons and $^{1}H_2O$. The reduction in the peak intensity of *KP*-PmrD amide resonances in complex with non-activated (Fig. 6A) or BeF_3^--activated PmrA$_N$ (Fig. 6B) were quantified and compared to results from the control experiment.

First, we set the irradiation center at 4.06 ppm. In the absence of BeF_3^- (Fig. 6A), only the intensities of the cross peaks of Leu26 at loop 2 and Ala51 at loop 4 were predominantly decreased in the saturation condition. In the presence of BeF_3^- (Fig. 6B), more amide resonances, such as Trp4, Glu27, Met28, Leu45, Thr46, Ala51, Asn58, Thr69 and His70, showed low intensity ratios as compared to those in the absence of BeF_3^-. These results were shown in a ribbon structure of *KP*-PmrD, with the intensity ratios coded by a color gradient (Fig. 6C and D). The binding sites on *KP*-PmrD with non-activated PmrA$_N$ were located at the N terminus of β3 and loop 4 only and expanded to one face of the β-barrel mainly consisting of the N terminus of β1, C terminus of β2, N terminus of β3, whole β4, loop 4, and loop 6 (Fig. 6D) when in complex with BeF_3^--activated PmrA$_N$.

As well, we examined the saturation transfer with irradiation center at 4.26 ppm (data not shown). The results generally agreed with those observed with the irradiation center at 4.06 ppm.

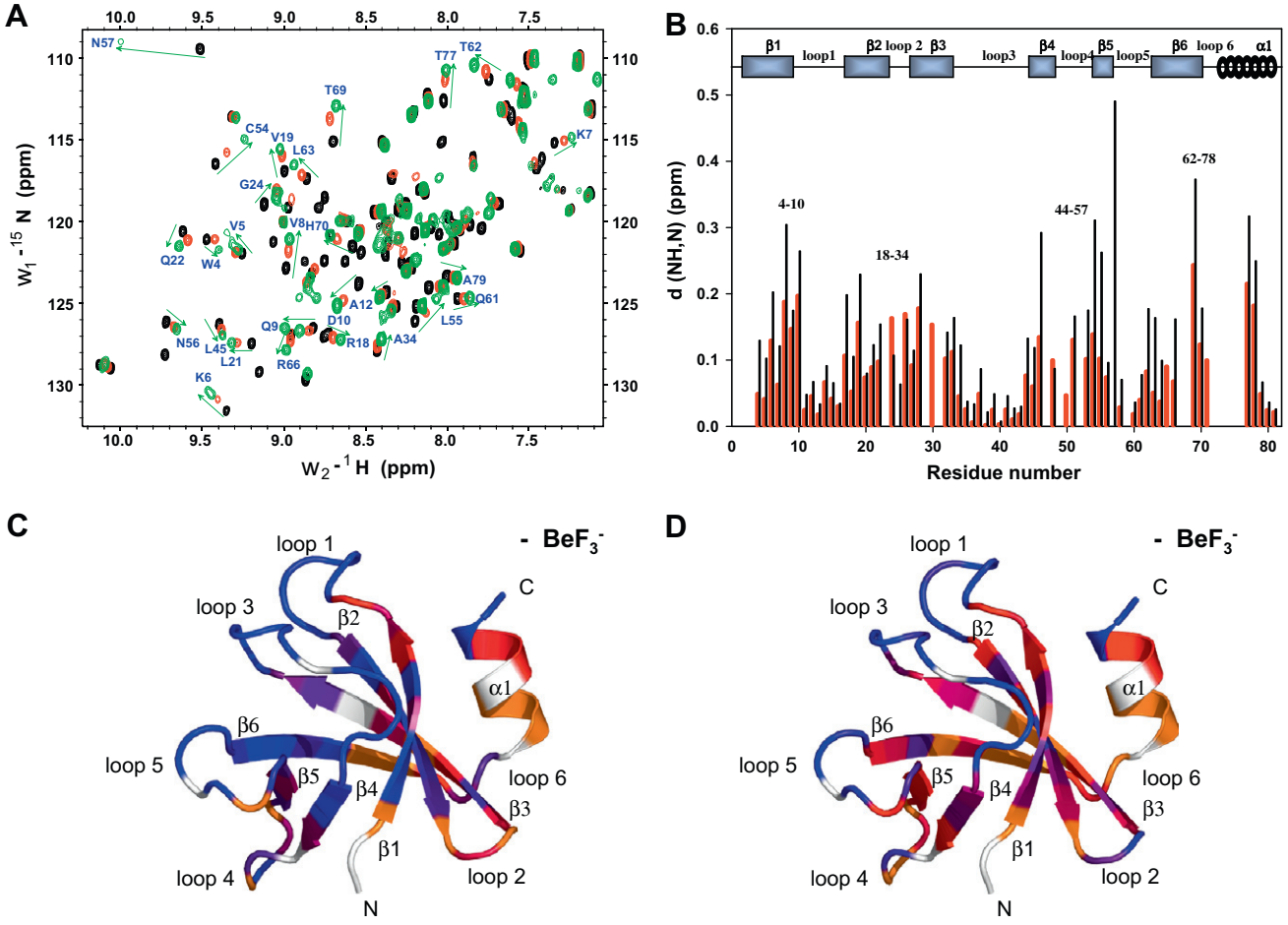

Fig. 5. Protein–protein interactions by NMR and surface mapping of *KP*-PmrD binding with non-activated and BeF_3^--activated $PmrA_N$. (A) Overlay of the ^1H, ^{15}N-HSQC (800 MHZ) of ^{15}N, ^2H-labeled *KP*-PmrD in its free form (black) and bound form with $PmrA_N$ (molar ratio 1:2) without (red) or with (green) BeF_3^-. The backbone assignments are shown for the residues that exhibit significant chemical shift perturbations. The peak shifts are indicated by arrows. (B) Correlation of chemical shift perturbations versus residues in *KP*-PmrD with the addition of $PmrA_N$ in the absence (red bars) and presence (black bars) of BeF_3^-. Chemical shift changes in *KP*-PmrD because of the binding of $PmrA_N$ without (C) and with (D) BeF_3^- were mapped onto a ribbon diagram. A color gradient from blue to red indicates a 0.05- to 0.2-ppm change. Residues whose resonances disappeared because of peak broadening or that are unassigned are orange or white, respectively.

Table 2
Dissociation constants* of *KP*-PmrD in complex with inactive $PmrA_N$.

Residue	Dissociation constant (μM)
Lys6	204.9
Val8	285.2
Asp10	232.8
Val19	340.8
Gln22	225.3
Gly24	192.2
Thr62	144.7
Thr69	302.1
Thr77	201.0
Averaged K_D	±48.5 (μM)

* The dissociation constants were given for the nine amino acid residues showing the most prominent Δδ upon *KP*-PmrD titration with $PmrA_N$ in the absence of BeF_3^-).

3.7. In vivo polymyxin B susceptibility assay of the site-directed mutagenesis on KP-PmrD verified saturation transfer data

In the *pmrD*-mediated pathway (Kato et al., 2007), the low magnesium signal is received by the TCS PhoPQ and passed to PmrAB via PmrD to allow the bacteria to become polymyxin resistant. To investigate the role of *KP*-PmrD in the regulatory architecture, a *pmrD* deletion mutant strain designated D2906 was generated, and its resistance to polymyxin B was determined. On challenge with increasing doses of polymyxin B, the wild-type strain showed no growth at concentrations >6 U/ml, whereas strain D2906 was totally eliminated on treatment with > 4 U/ml polymyxin B (data not shown). The result from treatment with 4 U/ml polymyxin B was shown in Fig. 7A, and the survival rate of the *pmrD* mutant strain D2906 is lower than that of its parental strain. pHY119, a plasmid carrying a functional *pmrD* gene, was introduced into strain D2906 and restored the resistance to almost 100%. Our results suggested that an intact *Klebsiella pmrD* gene is required for full resistance to polymyxin B under low-magnesium conditions, and introduction of multiple copies of *pmrD* significantly enhanced the bacterial resistance to the antimicrobial agent.

To further verify the results of saturation transfer experiments, we selected three residues (Leu26, Met28, and Thr46) with significant reduced intensity ratios and two residues (Thr77 and Asn78) showing small saturation transfer effects but large chemical shift perturbations for site-directed mutagenesis and polymyxin B susceptibility assay. As shown in Fig. 7B, the *K. pneumoniae* Δ*pmrD* strain carrying the control vector pRK415 was largely impaired in resistance to polymyxin B, whereas the strain carrying pRK415-

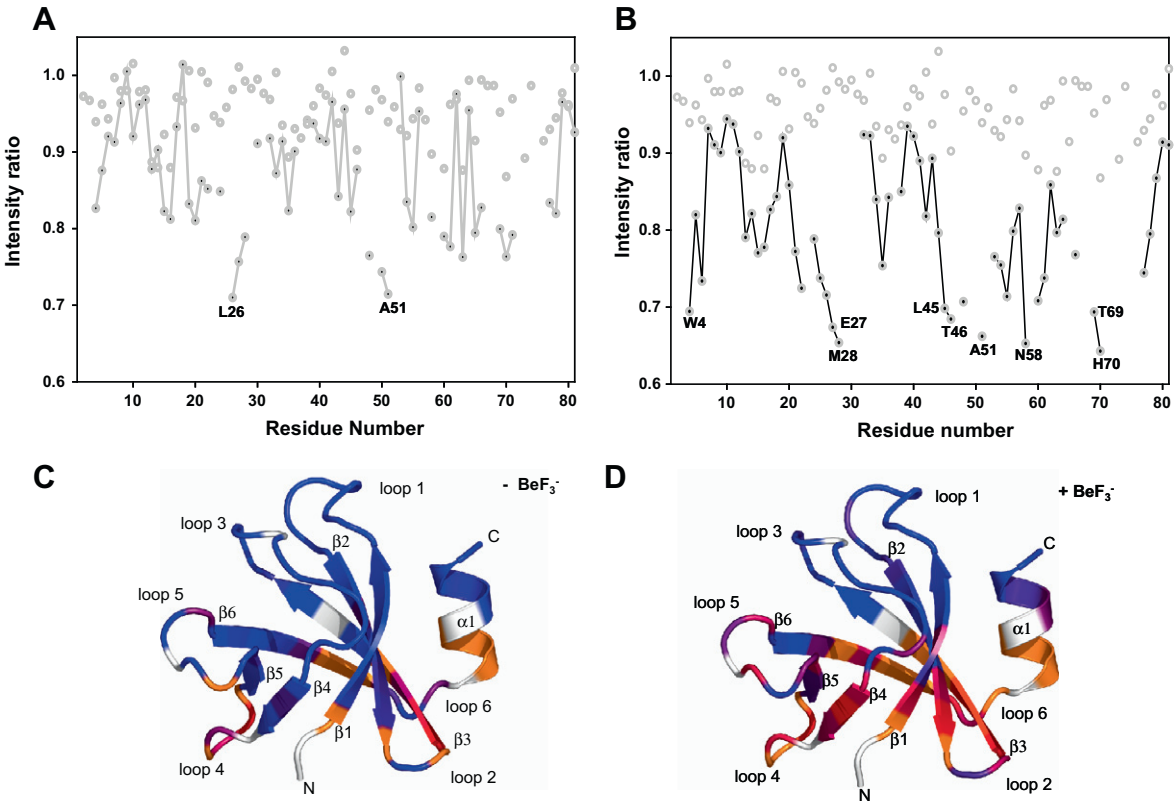

Fig. 6. Saturation transfer effects on *KP*-PmrD on binding to non-activated and BeF_3^--activated $PmrA_N$ (at a molar ratio of 2). The intensity ratio of the amide proton resonances, with and without irradiation of the aliphatic region, is plotted against the *KP*-PmrD residue number. The solid circles represent the saturation transfer experiment performed on ^2H, ^{15}N-labeled *KP*-PmrD bound to unlabeled $PmrA_N$ without (A) or with (B) BeF_3^-. The open circles represent a control experiment performed on the free ^2H, ^{15}N-labeled *KP*-PmrD. Saturation transfer effect because of the binding of $PmrA_N$ without (C) or with (D) BeF_3^- were mapped onto a ribbon diagram of *KP*-PmrD. A color gradient from blue to red indicates a 0.92 to 0.70 change of intensity ratio. Residues whose resonances disappeared or were unassigned are orange or white, respectively.

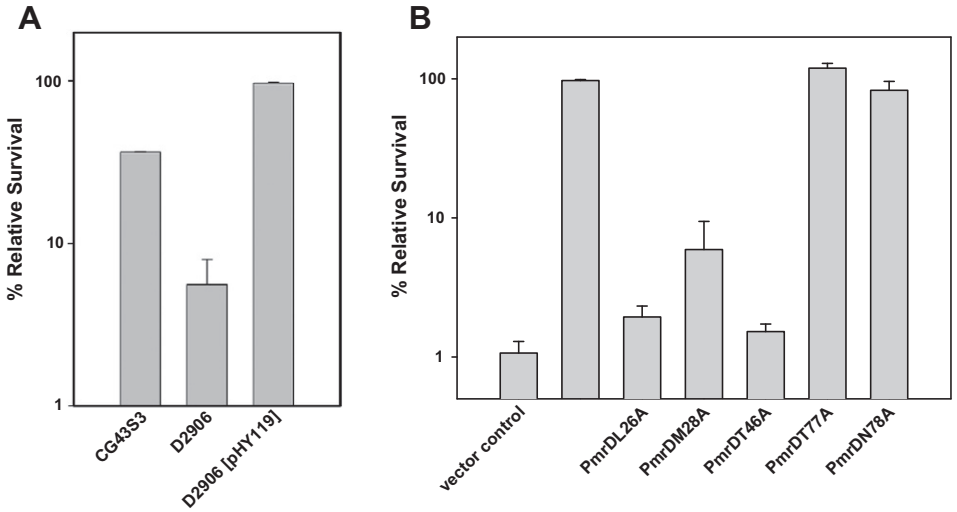

Fig. 7. Polymyxin B resistance assay of *K. pneumoniae* CG43S3, D2906 (Δ*pmrD*) and D2906 [pHY119] was performed with log-phased bacterial culture (A). Polymyxin B susceptibility assay of *K. pneumoniae* Δ*pmrD* mutant harboring different *pmrD* complementation plasmids (B). The *K. pneumoniae* transformants were grown to log-phase for the polymyxin B susceptibility assay. Shows the relative survival of strains carring pRK415 (vector control) or a pRK415-derived plasmid encoding the wild-type (PmrD) or PmrD with each point mutation on the challenge of 4 units/ml polymyxin B. The results are the averaged survival rates from triplicate samples. Error bar indicates the standard deviation. Saturation transfer experiments of three affected residues (Leu26, Met28, and Thr46) and two residues with large chemical shift perturbation at C-terminal α-helix (Thr77 and Asn78) but small saturation transfer effects were selected for assay.

PmrD encoding a wild-type PmrD exhibited almost 100% survival. The strain harboring the plasmid encoding PmrDL26A, PmrDM28A, or PmrD46A showed greatly reduced resistance to polymyxin B, which indicates that these residues were all involved in *KP*-PmrD-regulated polymyxin B resistance. This finding was consistent with the saturation transfer results. However, the strain carrying pRK415-PmrDT77A or -PmrDN78A remained resistant to polymyxin B, which indicates that the large chemical shift pertur-

bation on the C-terminal α-helix of *KP*-PmrD did not result from its direct contact with $PmrA_N$. In summary, our findings from *in vivo* polymyxin B susceptibility assay comparing the mutant plasmids encoding site-directed *KP*-PmrD mutants have further confirmed the results of saturation transfer experiments and indicated that the PmrD C-terminal α-helix may not be involved in direct binding with $PmrA_N$.

4. Discussion

Although the structures of several HKs, RRs, and their complexes have been determined (Casino et al., 2009; Francis et al., 2004; Zapf et al., 2000), the mechanism by which PmrD connects the two TCSs remains elusive, and little is known about the details of PmrD interaction with phospho-PmrA. In this study, we detected significant chemical shift perturbations of *KP*-PmrD on its binding to non-activated $PmrA_N$ (Fig. 5A, red). The averaged dissociation constant (~236 μM) is close to the dissociation constant of ~200 μM for the *E. coli* YojN histidine-phosphotransferase domain (Yoj-HPt) in complex with the non-activated receiver domain of RcsC (RcsC-PR) (Rogov et al., 2004). According to the titration profiles, *KP*-PmrD exhibits a fast exchange regime on binding with the non-activated $PmrA_N$ and a slow exchange regime with the BeF_3^--activated $PmrA_N$. The slow exchange regime is in agreement with a low off-rate value obtained from SPR, because the off rate (0.073 s^{-1}) is much smaller than the difference in chemical shift (e.g., ~120 Hz for Thr77) between the free and bound forms (Marintchev et al., 2007). Thus, the interaction strength between *KP*-PmrD and $PmrA_N$ is comparable on NMR and SPR analysis. At a molar ratio of 1:2, *KP*-PmrD showed larger chemical shift perturbations with BeF_3^--activated $PmrA_N$, which suggests a stronger interaction. This result is consistent with the observation that in the RcsC-PR domain, the interaction with the RcsD-HPt domain becomes stronger with the addition of Mg^{2+} and BeF_3^- (Rogov et al., 2006; Rogov et al., 2008). Also, our titration data suggest that the binding mode of *KP*-PmrD with non-activated $PmrA_N$ is similar to BeF_3^--activated $PmrA_N$ because the chemical shift changes in general are in the same direction and are smaller without BeF_3^- because of less binding. The affinity changes with or without BeF_3^- and leads to the different exchange regime in the NMR time scale. However, we could not identify the binding sites on *KP*-PmrD with the BeF_3^--activated $PmrA_N$ because the residues with large chemical shift differences lie in the core and several discontinuous surfaces of the protein.

To further investigate the interaction of *KP*-PmrD and $PmrA_N$, we performed saturation transfer experiments. In the absence of BeF_3^-, Leu26 and Ala51 were the most affected residues (Fig. 6A). However, Met28 and Ile65 were the most affected residues at a different irradiation frequency (data not shown). Surface structure analysis of *KP*-PmrD showed that Leu26 and Ala51 are close to Met28 and Ile65, respectively (Fig. S5), which indicates that the saturation transfer results are consistent, and the interface residues on *KP*-PmrD could be accurately determined. In the presence of BeF_3^-, several residues showed significantly reduced intensity ratios (Fig. 6B), which suggests a larger interacting surface between *KP*-PmrD and BeF_3^--activated $PmrA_N$. Mapping these affected residues plus the resonances that disappeared on the surface of *KP*-PmrD revealed a contiguous patch consisting of Trp3, Trp4, Ser23, Leu26, Glu27, Met28, Thr46, Leu48, Ala49, Asp50, Ala51, Arg52, Ile65, Asn67, Ala68, Thr69, His70, Tyr71, Ser73 and Glu74 (Fig. S5), which is likely the interacting surface with BeF_3^--activated $PmrA_N$. These residues were also found to exhibit large chemical shift perturbations (>0.1 ppm) on the formation of a complex. Thus, features of the protein–protein interaction between *KP*-PmrD and $PmrA_N$ are well reflected in the mapping of the saturation transfer-affected residues. Electrostatic interactions play a vital stabilizing role and are important in initiating protein–protein interactions (Ivanova and Lu, 2008). The conserved Asp51 of PmrA is structurally surrounded by a cluster of acidic residues that results in a large negatively charged area on the protein surface (Fu et al., 2007). The basic residues in the *KP*-PmrD (PI = 7.8) are suggested to participate in the recognition of the phospho-aspartate in PmrA (Kato and Groisman, 2004). Consequently, five basic residues of *KP*-PmrD (Arg52, Lys64, Arg66, His70, and Arg75) were found to be located at or near the proposed $PmrA_N$ interacting surface on *KP*-PmrD. Among them, the positive-charge residue His70, which is replaced by a non-charged residue in *E. coli* PmrD (Ser70), showed the lowest intensity ratio in saturation transfer experiments. Besides, residue conservation has been suggested to be higher at protein binding sites than at other protein surface areas (Keskin et al., 2008). From the mapped binding site, as compared with *Salmonella* PmrD, *KP*-PmrD contains a cluster of sequence-conserved residues (Trp3, Leu26, Met28, Asp50, Ala51, and Ile65) located on the contiguous patch, so they might play important roles in mediating the interactions between *KP*-PmrD and phospho-PmrA. Three of these conserved residues show variances with *E. coli* PmrD (L26I, D50N, and I65V), which might lead to different functions for the highly divergent PmrD proteins. Furthermore, a hydrophobic patch formed by Leu26, Met28, and Trp3 is located in the center of the interface (Fig. S5). Consistently, cross peaks on two residues (Trp3Nε1 and Ile65) disappeared at the beginning when titrating ^{15}N, ^{2}H-labeled *KP*-PmrD with $PmrA_N$ (data not shown), which suggests that side chains of these two residues probably contribute to $PmrA_N$ binding. From the above results and the stoichiometry of *KP*-PmrD binding to $PmrA_N$, we suggest a recognition mode that involves two *KP*-PmrD proteins in complex with the BeF_3^--activated-$PmrA_N$ dimer (Fig. 8). In the model structure of BeF_3^--activated-$PmrA_N$ dimer, the phosphoryl analog, BeF_3^- (shown as magenta sticks in Fig. 8) is located at an exposed surface, where *KP*-PmrD should protect and accordingly is highly possible to be the interaction surface on PmrA. For *KP*-PmrD, we propose that the C-terminal helices of two PmrD proteins may interact with each other in complex with the activated-$PmrA_N$ dimer. This orientation explains why two residues on the C-terminal α-helix (Thr77 and Asn78) and nearby residues on the consecutive beta strands β1 to β3 (e.g., Val8, Asp10, Val19, and Glu33) of *KP*-PmrD show large chemical shift perturbations (Fig. 5B and D) but are far away from the interactions surfaces identified by saturation transfer experiments (Fig 6B and D). As well, a high degree of shape complementation has been found necessary to form specific polar interactions, such as hydrogen bonds and salt bridges, which fulfill the requirements for much of the complexity of protein–protein interactions (Reichmann et al., 2007). However, it is also possible that the chemical shift perturbations of these residues come from structural rearrangement upon binding but not interactions between two *KP*-PmrD proteins. The determination of PmrD–$PmrA_N$ complex structure is currently proceeding to verify their interaction mode.

We showed that *KP*-PmrD can inhibit the dephosphorylation of PmrA by PmrB, which is similar to *Salmonella* PmrD but not *E. coli* PmrD. Therefore, knowing the structural basis of PmrDs from different bacteria possessing distinct functions is of interest. Detailed comparisons of structures showed that the C-terminal α-helix is shorter in *KP*-PmrD than that in *E. coli* (Fig. S6A). Furthermore, *E. coli* PmrD HZ3 of Lys86 in the C-terminal α-helix formed a hydrogen bond with the carbonyl oxygen of Gln13 in the loop 1 region, and a number of non-bonded interactions exist between loop 1 and the C-terminal α-helix. A salt bridge was found between C-terminal carboxyl group of Gln88 and Lys12 at loop 1, and the dynamics of the C-terminal α-helix of *E. coli* PmrD remained stable during molecular dynamic trajectory (Tatsis et al., 2009). However,

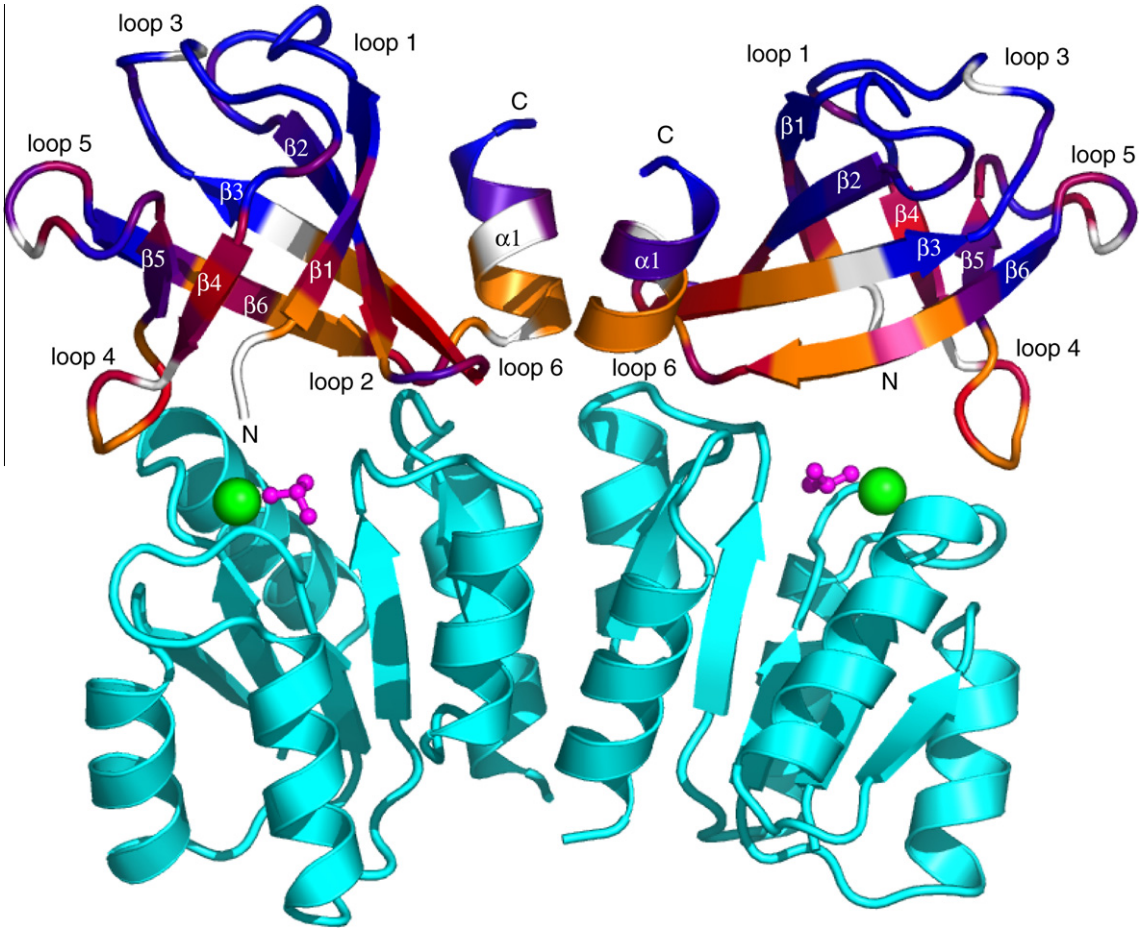

Fig. 8. The phospho-PmrA recognition mode of *KP*-PmrD, which involves two *KP*-PmrD proteins in complex with an activated-$PmrA_N$ dimer, was revealed from saturation transfer experiments, and the color gradient is the same as in Fig. 6D. We modeled the ribbon structure of the $PmrA_N$ dimer using the crystal structure of PhoP from *E. coli* in the presence of BeF_3^- (PDB entry 2PKX) (in pale green). The noncovalent BeF_3^- and Mg^{2+} within the active site are shown as pink stick and cyan spheres, respectively. The flexible C-terminal α-helix of *KP*-PmrD could collide with the C-terminal α-helix of another *KP*-PmrD if they were docked on the same $PmrA_N$ dimer with twofold symmetry, which explains why two resonances on C-terminal α-helix (Thr77 and Asn78) and nearby residues on the consecutive beta strands 1-2-3 (e.g., Val8, Asp10, Val19, and Glu33) of *KP*-PmrD showed large chemical shift perturbation but small saturation transfer effects.

we did not observe hydrogen bond, non-bonded interactions or salt bridges between loop 1 and the C-terminal α-helix in *KP*-PmrD, which indicates a more flexible C-terminal α-helix. To confirm this observation, we performed a backbone dynamics study of *KP*-PmrD to provide information about the flexibility of each region in solution. Most of the residues in the β-strands had HX-NOEs > 0.7, but residues in C-terminal α-helix possessed surprisingly lower HX-NOEs (Fig. S6B), which suggests that they are quite flexible. Accordingly, the short C-terminal α-helix of *KP*-PmrD is more flexible than that of *E. coli* PmrD, and the structural dissimilarity provides hints to explain different functions of PmrD proteins.

In conclusion, we present the solution structure of *KP*-PmrD and show that it can inhibit the dephosphorylation of phospho-PmrA. *KP*-PmrD interaction with non-activated or BeF_3^--activated $PmrA_N$ significantly differed. The binding stoichiometry of the two proteins was suggested to be 1:1, and the two proteins seem to form a complex comprising a $PmrA_N$ dimer bound to 2 molecules of *KP*-PmrD. NMR titrations suggested that the binding mode of *KP*-PmrD with non-activated $PmrA_N$ is similar to that with BeF_3^--activated $PmrA_N$. A combination of saturation transfer and chemical shift perturbation experiments were used to separate the direct intermolecular contacts from the effects due to conformational rearrangement and suggested the phospho-$PmrA_N$ recognition mode on *KP*-PmrD. *In vivo* polymyxin B susceptibility assay of the site-directed mutagenesis on *KP*-PmrD confirmed the saturation transfer results. The phospho-$PmrA_N$ binding mode on *KP*-PmrD provided here should be useful in deriving the *KP*-PmrD binding residues on $PmrA_N$. This is the first report of the binding strength and phospho-PmrA recognition mode of the connector protein PmrD. Our study furthers the understanding of selective binding for PmrD proteins that regulate TCSs for better adaptation to rapid environmental changes.

Acknowledgments

This work was supported by grants from Academia Sinica (94F001-2) and the National Science Council (NSC 97-2311-B-001-013-MY3), Taiwan, ROC. The NMR spectra were obtained at the High-field Biomacromolecular NMR Core Facility at Academia Sinica, supported by the National Science and Technology Program for Medical Genomics. We also thank Dr. Wen-Jin Wu for help in modifying the pulse program in saturation transfer experiments and Laura Smales for copyediting the manuscript.

Appendix A. Supplementary data

Supplementary data associated with this article can be found, in the online version, at doi:10.1016/j.jsb.2010.06.007.

References

Aguirre, A., Lejona, S., Vescovi, E.G., Soncini, F.C., 2000. Phosphorylated PmrA interacts with the promoter region of ugd in *Salmonella enterica* serovar typhimurium. J. Bacteriol. 182, 3874–3876.

Anglister, J., Grzesiek, S., Ren, H., Klee, C.B., Bax, A., 1993. Isotope-edited multidimensional NMR of calcineurin B in the presence of the non-deuterated detergent CHAPS. J. Biomol. NMR 3, 121–126.

Bruce, A.J., Richard, A.B., 1994. NMR view: a computer program for the visualization and analysis of NMR data. J. Biomol. NMR V4, 603–614.

Campos, M.A., Vargas, M.A., Regueiro, V., Llompart, C.M., Alberti, S., Bengoechea, J.A., 2004. Capsule polysaccharide mediates bacterial resistance to antimicrobial peptides. Infect. Immun. 72, 7107–7114.

Casino, P., Rubio, V., Marina, A., 2009. Structural insight into partner specificity and phosphoryl transfer in two-component signal transduction. Cell 139, 325–336.

Cho, H., Wang, W., Kim, R., Yokota, H., Damo, S., Kim, S.H., Wemmer, D., Kustu, S., Yan, D., 2001. BeF(3)(−) acts as a phosphate analog in proteins phosphorylated on aspartate: structure of a BeF(3)(−) complex with phosphoserine phosphatase. Proc. Natl. Acad. Sci. USA 98, 8525–8530.

Delaglio, F., Grzesiek, S., Vuister, G.W., Zhu, G., Pfeifer, J., Bax, A., 1995. NMRPipe: a multidimensional spectral processing system based on UNIX pipes. J. Biomol. NMR 6, 277–293.

Francis, N.R., Wolanin, P.M., Stock, J.B., Derosier, D.J., Thomas, D.R., 2004. Three-dimensional structure and organization of a receptor/signaling complex. Proc. Natl. Acad. Sci. USA 101, 17480–17485.

Fu, W., Yang, F., Kang, X., Zhang, X., Li, Y., Xia, B., Jin, C., 2007. First structure of the polymyxin resistance proteins. Biochem. Biophys. Res. Commun. 361, 1033–1037.

Gabriel, C., Frank, D., Ad, B., 1999. Protein backbone angle restraints from searching a database for chemical shift and sequence homology. J. Biomol. NMR V13, 289–302.

Goddard, T.D., Kneller, D.G. 2001. SPARKY 3.

Groisman, E.A., 2001. The pleiotropic two-component regulatory system PhoP-PhoQ. J. Bacteriol. 183, 1835–1842.

Groisman, E.A., Kayser, J., Soncini, F.C., 1997. Regulation of polymyxin resistance and adaptation to low-Mg2+ environments. J. Bacteriol. 179, 7040–7045.

Hoch, J.A.a.S.T.J. (Ed.), 1995. Two-Component Signal Trasduction. ASM Press.

Huang, H., Milojevic, J., Melacini, G., 2008. Analysis and optimization of saturation transfer difference NMR experiments designed to map early self-association events in amyloidogenic peptides. J. Phys. Chem. B 112, 5795–5802.

Ivanova, E., Lu, H., 2008. Allosteric and electrostatic protein–protein interactions regulate the assembly of the heterohexameric Tim9–Tim10 complex. J. Mol. Biol. 379, 609–616.

Kato, A., Groisman, E.A., 2004. Connecting two-component regulatory systems by a protein that protects a response regulator from dephosphorylation by its cognate sensor. Genes Dev. 18, 2302–2313.

Kato, A., Mitrophanov, A.Y., Groisman, E.A., 2007. A connector of two-component regulatory systems promotes signal amplification and persistence of expression. Proc. Natl. Acad. Sci. USA 104, 12063–12068.

Kay, L.E., 1995. Pulsed field gradient multi-dimensional NMR methods for the study of protein structure and dynamics in solution. Prog. Biophys. Mol. Biol. 63, 277–299.

Keen, N.T., Tamaki, S., Kobayashi, D., Trollinger, D., 1988. Improved broad-host-range plasmids for DNA cloning in gram-negative bacteria. Gene 70, 191–197.

Keskin, O., Gursoy, A., Ma, B., Nussinov, R., 2008. Principles of protein–protein interactions: what are the preferred ways for proteins to interact? Chem. Rev. 108, 1225–1244.

Kox, L.F., Wosten, M.M., Groisman, E.A., 2000. A small protein that mediates the activation of a two-component system by another two-component system. EMBO J. 19, 1861–1872.

Lai, Y.C., Peng, H.L., Chang, H.Y., 2003. RmpA2, an activator of capsule biosynthesis in *Klebsiella pneumoniae* CG43, regulates K2 cps gene expression at the transcriptional level. J. Bacteriol. 185, 788–800.

Marintchev, A., Frueh, D., Wagner, G., 2007. NMR methods for studying protein–protein interactions involved in translation initiation. Methods Enzymol. 430, 283–331.

Mitrophanov, A.Y., Groisman, E.A., 2008. Signal integration in bacterial two-component regulatory systems. Genes Dev. 22, 2601–2611.

Prince, S.E., Dominger, K.A., Cunha, B.A., Klein, N.C., 1997. *Klebsiella pneumoniae* pneumonia. Heart Lung 26, 413–417.

Reichmann, D., Rahat, O., Cohen, M., Neuvirth, H., Schreiber, G., 2007. The molecular architecture of protein–protein binding sites. Curr. Opin. Struct. Biol. 17, 67–76.

Rogov, V.V., Bernhard, F., Lohr, F., Dotsch, V., 2004. Solution structure of the *Escherichia coli* YojN histidine-phosphotransferase domain and its interaction with cognate phosphoryl receiver domains. J. Mol. Biol. 343, 1035–1048.

Rogov, V.V., Rogova, N.Y., Bernhard, F., Koglin, A., Lohr, F., Dotsch, V., 2006. A new structural domain in the *Escherichia coli* RcsC hybrid sensor kinase connects histidine kinase and phosphoreceiver domains. J. Mol. Biol. 364, 68–79.

Rogov, V.V., Schmoe, K., Lohr, F., Rogova, N.Y., Bernhard, F., Dotsch, V., 2008. Modulation of the Rcs-mediated signal transfer by conformational flexibility. Biochem. Soc. Trans. 36, 1427–1432.

Roman, A.L., Rullmann, J.A.C., Malcolm, W.M., Robert, K., Janet, M.T., 1996. AQUA and PROCHECK-NMR: programs for checking the quality of protein structures solved by NMR. J. Biomol. NMR V8, 477–486.

Sambrook, J., Fritsch, E.F., Maniatis, T., 1989. Molecular Cloning: A Laboratory Manual, 2nd ed. Cold Spring Habor Laboratory, Cold Spring Harbor, NY.

Stock, A.M., Robinson, V.L., Goudreau, P.N., 2000. Two-component signal transduction. Annu. Rev. Biochem. 69, 183–215.

Takahashi, H., Nakanishi, T., Kami, K., Arata, Y., Shimada, I., 2000. A novel NMR method for determining the interfaces of large protein–protein complexes. Nat. Struct. Biol. 7, 220–223.

Tatsis, V.A., Tsoulos, I.G., Krinas, C.S., Alexopoulos, C., Stavrakoudis, A., 2009. Insights into the structure of the PmrD protein with molecular dynamics simulations. Int. J. Biol. Macromol. 44, 393–399.

Winfield, M.D., Groisman, E.A., 2004. Phenotypic differences between *Salmonella* and *Escherichia coli* resulting from the disparate regulation of homologous genes. Proc. Natl. Acad. Sci. USA 101, 17162–17167.

Wishart, D.S., Sykes, B.D., 1994. The 13C chemical-shift index: a simple method for the identification of protein secondary structure using 13C chemical-shift data. J. Biomol. NMR 4, 171–180.

Wosten, M.M., Kox, L.F., Chamnongpol, S., Soncini, F.C., Groisman, E.A., 2000. A signal transduction system that responds to extracellular iron. Cell 103, 113–125.

Wurgler-Murphy, S.M., Saito, H., 1997. Two-component signal transducers and MAPK cascades. Trends Biochem. Sci. 22, 172–176.

Yan, D., Cho, H.S., Hastings, C.A., Igo, M.M., Lee, S.Y., Pelton, J.G., Stewart, V., Wemmer, D.E., Kustu, S., 1999. Beryllofluoride mimics phosphorylation of NtrC and other bacterial response regulators. Proc. Natl. Acad. Sci. USA 96, 14789–14794.

Zapf, J., Sen, U., Madhusudan, Hoch, J.A., Varughese, K.I., 2000. A transient interaction between two phosphorelay proteins trapped in a crystal lattice reveals the mechanism of molecular recognition and phosphotransfer in signal transduction. Structure 8, 851–862.